Atinafu *et al. Biochar* (2025) 7:18
https://doi.org/10.1007/s42773-024-00396-1

Biochar

ORIGINAL RESEARCH Open Access

Insights into the effects of biomass feedstock and pyrolysis conditions on the energy storage capacity and durability of standard biochar-based phase-change composites

Dimberu G. Atinafu[1], Ji Yong Choi[1], Jihee Nam[1], Yujin Kang[1] and Sumin Kim[1*]

Abstract

Material selection and production conditions are imperative for determining the functional performances of composite materials. Phase-change composites obtained from phase-change materials (PCMs) and supporting matrices exhibit high thermal energy storage density. They are used to overcome the intermittency issues of wind and solar energy, as well as to reduce waste heat dissipation to the environment. However, the large-scale utilization of composite and pristine materials has severe drawbacks, primarily stemming from the complex fabrication routes of the encapsulating agents, leakage, and inadequate thermal stability. In this study, biochar-based phase-change composites were fabricated using vacuum infiltration techniques, and the effects of biomass feedstock and pyrolysis temperature on the performance of the composite were elucidated using different types of biowastes and temperatures. This approach has several advantages, including facile production techniques, low-cost carbon sources, and environmental friendliness. The PCM adsorption ratio of biochars derived from rice husk (RH) and Miscanthus straw linearly correlated with the pyrolysis temperature (550–700 °C), while RH700 resulted in a composite with a high enthalpy per unit mass of hexadecane (HXD) in RH700/HXD (250.9 J g^{-1}) owing to the high surface area of RH700 (74.66 m^2 g^{-1}). The crystalline temperature increased slightly from 10.7 °C in RH550/HXD to 10.9 °C in RH700/HXD, suggesting improved molecular motion and crystal growth of HXD. Wheat straw biomass pyrolyzed at a low temperature (550 °C), displaying a reduced surface area at 700 °C (7.35 m^2 g^{-1}) and exhibiting the lowest energy storage density. The latent heat efficiency reached 99.5–100%, where RH700/HXD exhibited 100% efficiency. The composites demonstrated strong leakage resistance at high heating temperatures (60 °C, above the melting temperature of HXD), good chemical compatibility between the biochar and HXD, and high durability after 500 thermal cycles. Therefore, the extent of PCM loading and energy storage density improvements primarily depends on the pyrolysis conditions, feedstock used, and pore size distribution of the biochar samples. This research provides insights into the fabrication of phase-change composites and optimization of the carbonization process of different biomasses used for thermal management applications, such as building energy savings.

Highlights

- Different biochars were utilized to adsorb hexadecane and fabricate high-performance composite materials.
- Influence of feedstocks and pyrolysis temperature of biochar on thermal performance were investigated.
- Composites showed high enthalpy efficiency of 99.7–100% and durability after 500 thermal cycles.

*Correspondence:
Sumin Kim
kimsumin@yonsei.ac.kr
Full list of author information is available at the end of the article

Keywords Biomass, Biochar, Pyrolysis temperature, Thermal energy storage, Durability

Graphical Abstract

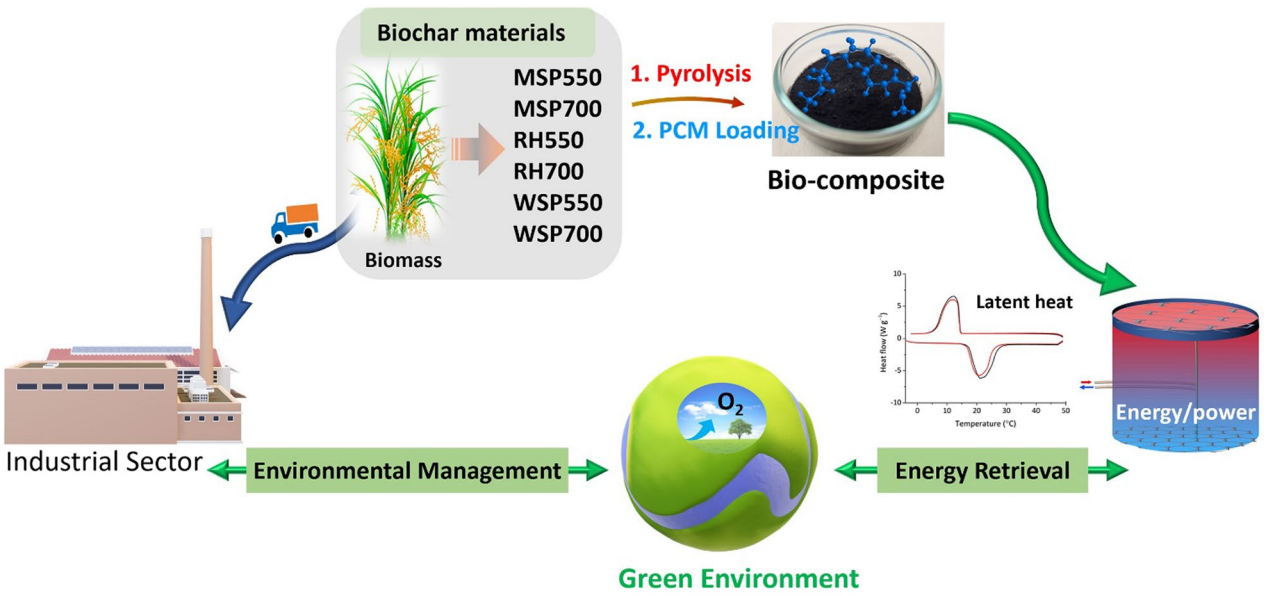

1 Introduction

Rapid population growth, industrialization, and global warming have necessitated the development of eco-friendly energy infrastructures. Hence, the development of renewable energy has received significant consideration owing to the depletion of fossil precursors, such as coal and other fossil fuels. Thermal energy storage using phase-change materials (PCMs) can potentially mitigate intermittency issues associated with wind and solar energy (Li et al. 2023a; b; Matuszek et al. 2023). PCMs, such as organic (e.g., paraffin, fatty alcohols, glycols, fatty acids, and their derivatives) and inorganic (e.g., salt hydrates, inorganic salts, and metals) materials, are employed in diverse thermal management systems, including solar heating systems, electronic thermal management, infrared stealth and thermal camouflage, and built environments (Ali et al. 2024; Freeman et al. 2023; Jing et al. 2023). Organic PCMs provide a notable platform for energy storage/release and related applications owing to their commercial availability, biocompatibility, low cost, low environmental impact, and high energy storage density (Qiu et al. 2020).

Nevertheless, intrinsic leakage problems and insufficient heat transfer performance (0.1–1 $W m^{-1} K^{-1}$) severely impede the direct utilization of these materials. These challenges are frequently addressed through the introduction of inorganic supporting materials, such as carbon nanotubes (CNTs), graphene-based materials, and carbon nitride (Al-Ahmed et al. 2021; Hekimoğlu et al. 2021c; Yu et al. 2024). Therefore, there have been extensive reports on the design of shape-stable phase-change composites for different thermal management applications (Singh et al. 2022). Kong et al. (2021) introduced paraffin wax into mesoporous polydivinylbenzene nanotubes. The resulting composite exhibited improved shape stability, electrothermal energy conversion efficiency (89.6%), and melting enthalpy (145.7 J g^{-1}). Li et al. (2023a; b) prepared reduced-graphene-oxide sheets using hydrazine for the development of paraffin-based composites. The composite demonstrated high photothermal conversion efficiency (81.6%), exceptional electromagnetic shielding effectiveness, and flame retardancy. Despite these achievements, the large-scale fabrication of shape-stable PCMs is restricted owing to the difficult preparation processes for supporting materials and environmentally unfriendly and costly raw materials. Moreover, unsatisfactory thermal durability during the phase-transition process and optimization of

the charging/discharging performance of PCMs remain practical challenges. Therefore, it is crucial to design an eco-friendly and commercially available PCM support (in this case, plant-based materials) to enable the production of high-performance composite materials and scalable thermal storage and management.

In this study, we fabricated phase-change composites based on hexadecane (HXD) and biowaste-derived biochar with high energy storage density. Biochar, found from the thermochemical transformation of biomaterial waste, is a carbon-rich material used in various applications, such as CO_2 uptake (Igalavithana et al. 2020; Yuan et al. 2024), building materials (Zhang et al. 2022b), catalysis in biorefineries (Yuan et al. 2023), electrochemical energy transformation and storage (Zeng et al. 2023), wastewater remediation (Foong et al. 2024), and soil amendment (Kalu et al. 2024). It is currently used as a PCM support in renewable energy development applications (Liang et al. 2023). For example, Yadav et al. (2024) utilized wheat husk-derived microparticles as solid supports to stabilize polyethylene glycol. The resulting composite exhibited high heat storage efficiency (3.99) and durability. In addition, polyethylene glycol infiltrated into nanosilver-integrated grapefruit peel-based porous carbon, resulting in a heating enthalpy of 134.1 J g^{-1} and improved thermal stability (Xie et al. 2024). However, the performance of biochar may depend primarily on factors such as its microstructure, morphology, raw materials used, and preparation parameters (e.g., pyrolysis temperature), which Xiong et al. (2022) mentioned as a limitation of their recent report on garlic-stem-biochar-based paraffin wax composites. In contrast, biochar derived from diverse biomass feedstocks possesses unique structural features, including the surface wettability of carbon materials and textural properties (e.g., surface area and pore channels), which significantly influence the advancement of biochar-based applications (Liu et al. 2015; Tomczyk et al. 2020). To the best of our knowledge, a simultaneous investigation into the influence of feedstock type, carbonization temperature, and biochar structural properties on the thermal characteristics (e.g., enthalpy and phase-transition temperature) of biochar-based phase-change composites is lacking. Accordingly, in this study, different biowaste-derived standard biochars (wheat straw, Miscanthus straw, and rice husk (RH) biochar) prepared at dissimilar temperatures (550 and 700 °C) were employed to encapsulate HXD. Because surface area is a prime indicator of biochar adsorption capacity, temperature is a vital factor in defining the textural properties of biochar during biochar production (Chun et al. 2004). Hence, this study examined the influences of biochar feedstocks and pyrolysis temperature on the energy storage density of biochar-based composites. This consideration has been lacking in previous investigations of biochar-based composites, which predominantly focused on the effects of PCMs functional groups (Lv et al. 2022). Additionally, the biochars explored in the present study revealed relatively different specific surface area ranges (7.3–75.0 m^2 g^{-1}), which were used to evaluate the effect of structural characteristics on the phase-change behavior of phase-change paraffin. Notably, a supporting material with excessively small pore sizes restricts the molecular motion of PCMs and affects the enthalpy storage (Weidner et al. 2019). Conversely, a pore size that is too large (mostly > 50 nm) increases susceptibility to leakage due to inadequate capillary forces to maintain the liquid PCM molecules (Qian et al. 2016). Moreover, the biochar developed without chemical activation and engineered with additives demonstrated high durability, retaining 87–91.8% of energy storage after 500 cycles. This contrasts with other biochars, such as bamboo-derived biochar engineered with CNTs, which maintained only 70% of PCM after 50 cycles (Atinafu et al. 2020). Furthermore, this study presents a cost-effective biochar with high thermal stability, promoting biocarbon in renewable energy storage and a circular economy, as illustrated in Fig. 1. Additionally, the as-synthesized biochar-based composite materials can be utilized as renewable energy storage materials in low-temperature applications, such as free-cooling ventilation systems in buildings.

2 Materials and methods

2.1 Materials

All chemicals used were of analytical grade. HXD (PARAFOL 16–97, 10 kg, purity > 97%) was acquired from Celsius Korea Inc., Seoul, South Korea, and produced by SASOL Germany Gmbh. Table 1 lists the thermal and physical characteristics of the pristine HXD.

2.2 Biochar production and properties

Biochar samples are standard materials provided by the UK Biochar Research Centre and are distributed for common global research and development purposes (Mašek et al. 2018b). The biomass feedstocks were pyrolyzed at 550 and 700 °C with a heating rate of up to 98 °C min^{-1}. Mašek et al. (2018a) from the UK Biochar Research Center documented detailed reactor configuration and standard biochar production. Typically, the feedstocks were firstly pelleted to reduce variation in physical form and further used to enhance handling and processing throughput owing to the even shape of pellets, and further used to provide similar visual morphology (Edeh et al. 2023). The standard kiln operation involves an initial nitrogen purge of the entire system during the heating process to reach the target temperature.

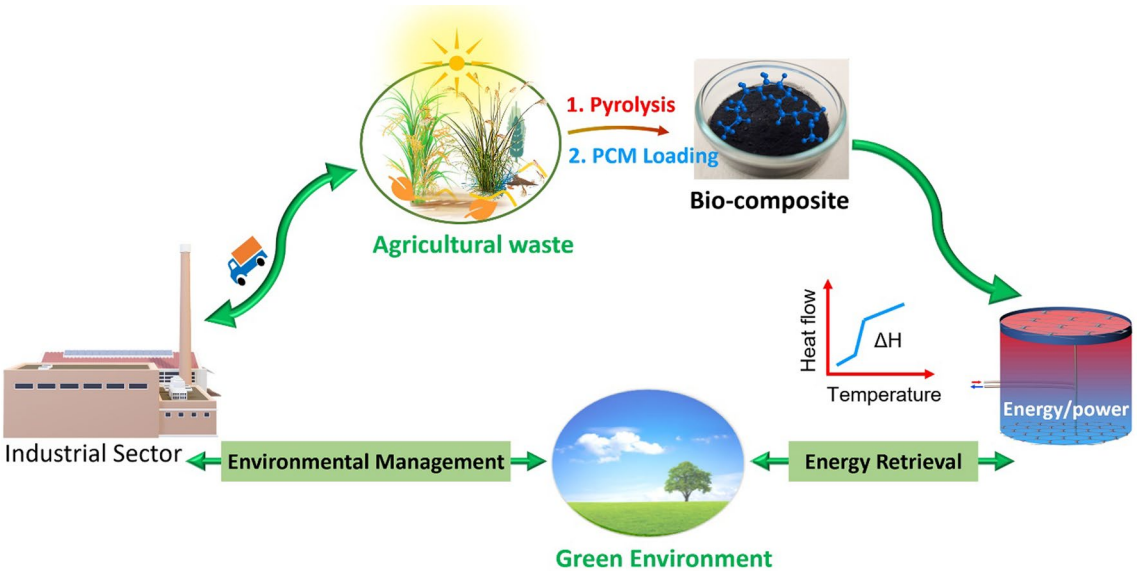

Fig. 1 Role of biochar in renewable energy storage and enabling a circular carbon economy

Table 1 Thermal and physical characteristics of pristine hexadecane

Property	Value
Molecular formula	CH_3–$(CH_2)_{14}$–CH_3
Phase-transition temperature	18 °C
Specific heat capacity	2 kJ $(kg\ K)^{-1}$
Heat transfer property	0.2 W $(m\ K)^{-1}$
Flash point	136 °C
Density (liquid at 25 °C)	0.77 g cm^{-3}

Subsequently, the feedstock was fed into the reactor at a specified rate using a horizontal screw feeder. The feedstocks then moved through the reactor, progressively undertaking drying, devolatilization, and carbonization. The resident time in the reactor was regulated by adjusting the speed and feed rate of the kiln. At the end, the product was detached from impurities (e.g., gases), cooled in a nitrogen-filled, water-jacketed screw without direct water contact, and transferred to a sealed drum, ensuring the biochar remains dry and protected from air and moisture. The essential properties of the biochar samples used to prepare the phase-change composites are presented in Table S1.

2.3 Preparation of paraffin-encapsulated biochar composites

The biochar samples (derived from the carbonization of Miscanthus straw, wheat straw, and RH biomass at different pyrolysis temperatures) were integrated with HXD using a vacuum encapsulation method, wherein liquid HXD was assorted with the biochar and shaken vigorously to enable infiltration into the biochar-supporting medium. The combined carbon–HXD sample was placed in a vacuum drying oven at 70 °C (above the melting temperature of bulk HXD) for 12 h. Extra liquid HXD was eliminated via filtration. The solid samples were subsequently dried at 70 °C for 12 h using a drying instrument. The dried materials obtained were seepage-resistant biochar-based composites and were represented as RH550/HXD, RH700/HXD, MSP550/HXD, MSP700/HXD, WSP550/HXD, and WSP700/HXD for the RH550, RH700, MSP550, MSP700, WSP550, and WSP700 derived materials, respectively. Figure 2 demonstrates the overall schematic of the preparation of the composite materials.

2.4 Characterization

The structural properties, such as the specific surface area (SSA), total pore volume ($V_{\text{total pore}}$), and pore size distribution, were characterized using the Brunauer–Emmett–Teller (BET) method, Barrett–Joyner–Halenda (BJH) model, and nitrogen adsorption–desorption isotherm analysis (ASiQwin; Quantachrome) at 77 K under a relative pressure (P/P_o) range of 0–1.0. The microstructures of the biochar and composite samples were evaluated using field-emission scanning electron microscopy (JEOL-7800 Prime). The chemical structure of the pristine materials and the chemical compatibility between HXD and the supporting carbon samples were examined using Fourier-transform infrared spectroscopy (FTIR; Nicolet 6700, Thermo Scientific, USA) over a wavenumber range of 500–4000 cm^{-1}. X-ray photoelectron

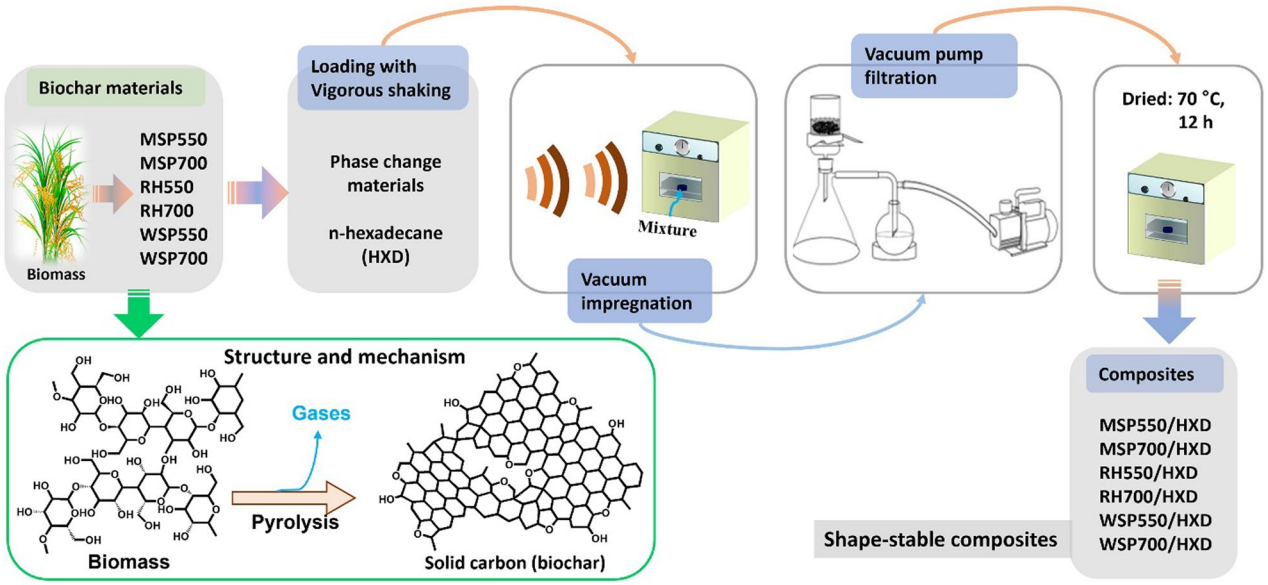

Fig. 2 Schematic of the fabrication of the biochar-based composite PCMs

spectroscopy (XPS) (Thermo Scientific Inc., U.K, X-ray source: Al K-alpha μ-focused monochromator (1486.6 eV) with variable spot size (30–400 μm in 5 μm steps) was employed to investigate the elemental composition of biochar materials and corresponding binding energies of specific elements. The crystallinity of the biochar was characterized using powder X-ray diffraction (XRD) patterns (D8 advance, Bruker, Germany) obtained with a Cu–K radiation source (λ = 1.541 Å) from 5° to 90° at a scanning rate of 10° min^{-1}. In addition, the degree of graphitization of biochar materials was evaluated using Raman spectrometer (Horiba Jobin Yvon) with laser, λ = 532 nm under a wavelength range of 4000–300 cm^{-1}. The thermal properties of HXD and the biochar–HXD composite were studied via differential scanning calorimetry (DSC; TA Instruments) from − 5 to 50 °C at a scanning rate of 10 °C min^{-1}. Furthermore, the thermal stability was evaluated through thermogravimetric analysis (TGA; Q5000, TA Instruments) from 20 to 600 °C at a scanning rate of 10 °C min^{-1} under a nitrogen gas flow. Meanwhile, the seepage-resistance capability of the biochar–HXD hybrid was assessed using a hot-stage digital camera approach by maintaining the sample at 60 °C (above the fusion point of HXD) for over 30 min. The durability was investigated using a rapid thermal cycler instrument (A300, LongGene) with 500 successive thermal cycles from room temperature (28 °C) to 50 °C. The thermal properties, including the phase-change enthalpy of the samples, were measured via DSC. The thermal conductivities of the as-prepared composite materials were investigated using a NETZSCH EPS (HFM 446) with a density of 26.0 kg m^{-3} and weight of 7.0 g. The measurement was performed thrice for each composite material with a mean deviation of ± 0.001 W m^{-1} K^{-1}. In addition, the thermal energy storage performance and homogeneity of the biochar–HXD composites were evaluated through dynamic thermal analysis using infrared thermography after 1 h of heating and 1 h of cooling in the range of 20–50 °C on an electric heating platform.

3 Results and discussion

3.1 Microstructure and textural features of biochars

The primary components of biomaterials (such as cellulose, hemicellulose, and lignin) can be employed as structural components with multiple microfibers and a high degree of polymerization for solid carbon (biochar) production. During carbonization, the biomass content and composition determine the diverse chemical, thermal, morphological, and structural characteristics of the solid carbon products, such as the SSA, pore volume, and pore diameter. Biomass is rich in fats and proteins that are not commonly considered during biochar fabrication owing to their heterogeneity and complex thermochemical conversion processes (Wang et al. 2021). Each biomass component requires a different pyrolysis temperature to produce solid carbon with the removal of CO, CO_2, H_2O, and certain hydrocarbons, as lignin requires a high pyrolysis temperature (Liu et al. 2015).

Figure 3a–f displays the scanning electron microscopy (SEM) images of the biochar materials, where different morphological structures were observed. Biochars obtained from Miscanthus straw and wheat straw

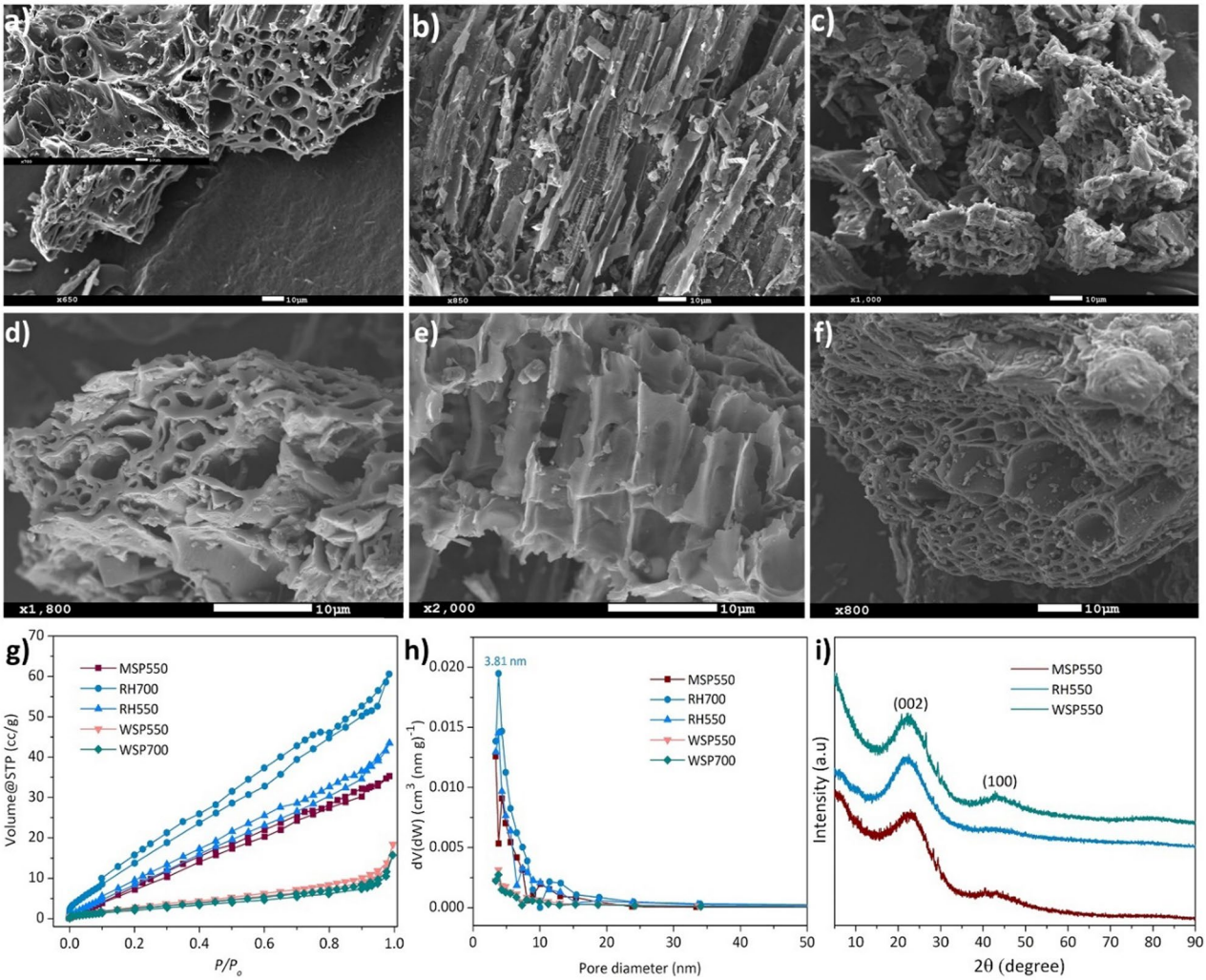

Fig. 3 Structural and thermal stability characteristics of the biomass-waste-derived biochars. SEM images of (**a**) MSP550, (**b**) RH550, (**c**) WSP550, (**d**) MSP700, (**e**) RH700, and (**f**) WSP700 are shown. **g** N_2 adsorption–desorption isotherms, **h** BJH pore-size distribution, and **i** XRD patterns of the biomass waste biochars

(MSP550, MSP700, WSP550, and WSP700) revealed randomly distributed pores within an irregular and interconnected hierarchical framework, with several surface pores of ~2 μm. In contrast, biochars derived from RH (RH550 and RH700) displayed an inherited structure from the biomass feedstocks, characterized by a regular microchannel network in an analogous direction, with an average width of ~3–5 μm and a plane surface (Fig. 3b, e). Additionally, RH constituents heteroatoms like nitrogen, confer the potential to advance the surface chemistry and improve the adsorption performances of biochars (Wan et al. 2020). These characteristics are essential for PCM adsorption, subsequently providing a high latent heat storage capacity. The nitrogen sorption isotherms and BJH pore-size distributions of the biochar materials are offered in Fig. 3g–h. The materials predominantly exhibited a type-IV isotherm with an H3 hysteresis adsorption–desorption isotherm observed between 0.5 and 0.9 P/P_o, demonstrating the existence of mesoporous carbon materials. All biochar samples exhibited similar features, with nearly no sorption isotherms at $P/P_o < 0.01$. Notably, WSP550 and WSP700 exhibited no apparent H3 loops between the sorption regions, confirming a tight network of mesopores and macropores. The obtained adsorption/desorption experiment revealed that WSP550 is distinctive because of an enhanced adsorption amount at a high P/P_o of 0.9–1.0, revealing the co-occurrence of meso–macro ordered pores (Liu et al. 2022a; Jin Zhao et al. 2017). This unique interconnectivity of the meso- and macropores is advantageous for the realization of ion

diffusion and adsorption, processes that are crucial for achieving high energy storage density (Yuan et al. 2017). Thus, RH700 had the highest BET SSA (74.66 m^2 g^{-1}), as well as BJH adsorption cumulative pore volume and pore diameter of 0.078 cm^3 g^{-1} and 3.42 nm, correspondingly. The BET SSAs of MSP550, RH550, WSP550, and WSP700 were 50.84, 54.91, 11.94, and 7.35 m^2 g^{-1}, respectively, with BJH adsorption cumulative pore volume values of 0.047, 0.058, 0.026, and 0.022 cm^3 g^{-1}. These values were substantially higher than those of currently documented biochar materials, such as walnut shell biochar (38.45 m^2 g^{-1}) (Hekimoğlu et al. 2021c), sugarcane bagasse biochar (17.78 m^2 g^{-1}) (Bordoloi et al. 2022), and phoenix leaf biochar (8.61 m^2 g^{-1}) (Lv et al. 2022), indicating the potential of the as-prepared materials for PCM adsorption. Among the biochar samples, WSP550 exhibited the highest BJH adsorption cumulative pore diameter (3.81 nm) and average pore diameter (9.53 nm), which is favorable for the even infiltration of PCM molecules into the inner channel of WSP500 and enhances the encapsulation rate of the PCM by WSP550 (Zhang et al. 2019). Contrary to other biochar materials that exhibited an improved SSA with increased temperature from 550 to 700 °C, WSP700 demonstrated the lowest textural properties, including the BET SSA and BJH adsorption cumulative volume, suggesting potential damage to certain physicochemical properties or fine-pore architectures at 700 °C (Chun et al. 2004). Thus, the wheat straw was nearly experiencing high carbonization at a temperature of ≥ 500 °C. The variation in the pore structure, including SSA, among the biochar matrices was presumably due to the unique lignocellulosic constituents (such as cellulose, hemicellulose, and lignin) of the biomass feedstocks (Edeh et al. 2023). Therefore, during pyrolysis, biomass with lesser cellulose and higher lignin contents results in biochar with higher porosity (Leng et al. 2021; Tomczyk et al. 2020). Notably, lignin, being more stable at higher temperatures than other lignocellulosic building blocks, is used to preserve porosity. In this context, RH700 and RH550 maintained their laterally oriented pores compared to those of MSP550, MSP700, WSP550, and WSP700, which displayed a more compact structure, as demonstrated in the SEM images (Fig. 3a–f). In addition, the biochar sample exhibited a major mesopore distribution at approximately 2.0–20 nm (Fig. 3h), which is promising for the fabrication of thermally stable energy-saving composite materials. Although the biochar showed a major mesopore proportion, micropores may still exist because nitrogen (77 K) adsorption is less reliable for the characterization of micropores, particularly narrow micropores (< 0.7 nm) (Zhang et al. 2022a).

Furthermore, XRD examination was conducted to evaluate the crystallinity of the biochar materials at low temperatures. Two distinctive and wide diffraction peaks were observed at approximately $2\theta = 23°$ and 43°, corresponding to the standard Bragg reflections (002) and (100) (Fig. 3i), respectively, confirming the amorphous nature of the biochar materials characterized by a low degree of graphitization.

Furthermore, the XPS survey was conducted to assess the differences in biochar materials elemental composition among the biochar materials. As shown in Fig. 4a, all the biochar materials showed carbon (C 1 s) and oxygen (O 1 s) with binding energies of approximately 283.4 eV and 531.3 eV, respectively, wherein C covered the dominant proportion over other elements. Meanwhile, other elements such as Si were predominantly detected in WSP550, WSP700, RH550, and RH700 samples at a binding energy of around 102.3–106.2 eV (Fig. 4a, circled with a dashed line). Such certain levels of metals and Si elements can contribute to preserving the microstructure of parent biomass materials and play an imperative role in the arrangement of C structure and stability of biochar materials (Guo & Chen 2014; Montoya et al. 2017). The deconvoluted C1s spectra revealed three major components at approximately 283.3–283.9 eV, 283.7–284.5 eV, and 286.0–287.3 eV, attributed to C=C/C–C, C–O, and O–C=O, respectively (Fig. S1). The O1s spectra also exhibited three deconvoluted components, occurring at around 529.7–530.7 eV, 530.0–532.2 eV, and 531.8–532.7 eV, corresponding to C=O, C–O, and O–C=O bonds (Fig. S2).

Additionally, the Raman spectra (Fig. 4b) displayed two prominent peaks situated at approximately 1343.1–1363.0 cm^{-1} and 1592.5–1598.3 cm^{-1}, equivalent to the D (defective carbon) and G (graphitic sp^2 carbon) bands, respectively. The relative intensity ratios between the D and G-bands ($I_D/I_{G)}$ ranged from 0.69 to 0.81, signifying a higher presence of amorphous carbon, as observed in XRD results. For instance, RH550 and MS550 showed an I_D/I_G value of 0.69 and 0.74, respectively, indicating a lower degree of defect and disorder in RH550 (Yang et al. 2022). With increasing pyrolysis temperature, the biochars revealed a red shift in the D bands (from 1361.7–1363.0 cm^{-1} at 550 to 1343.1–1346.3 cm^{-1} at 700 °C) and a blue shift in G bands (from 1592.5 to 1595.7 cm^{-1} at 550 °C to 1595.1–1598.3 cm^{-1} at 700 °C), suggesting that pyrolysis temperature significantly influences the degree of carbonaceous ordering and crystallinity (Haghighi Mood et al. 2022).

Furthermore, the FTIR absorption spectra revealed typical peaks of symmetric C–O, O–H, and aromatic C=C/C=O stretching vibrations at approximately 1090–1106, 3431, and 1575–1618 cm^{-1}, respectively (Fig. 4c).

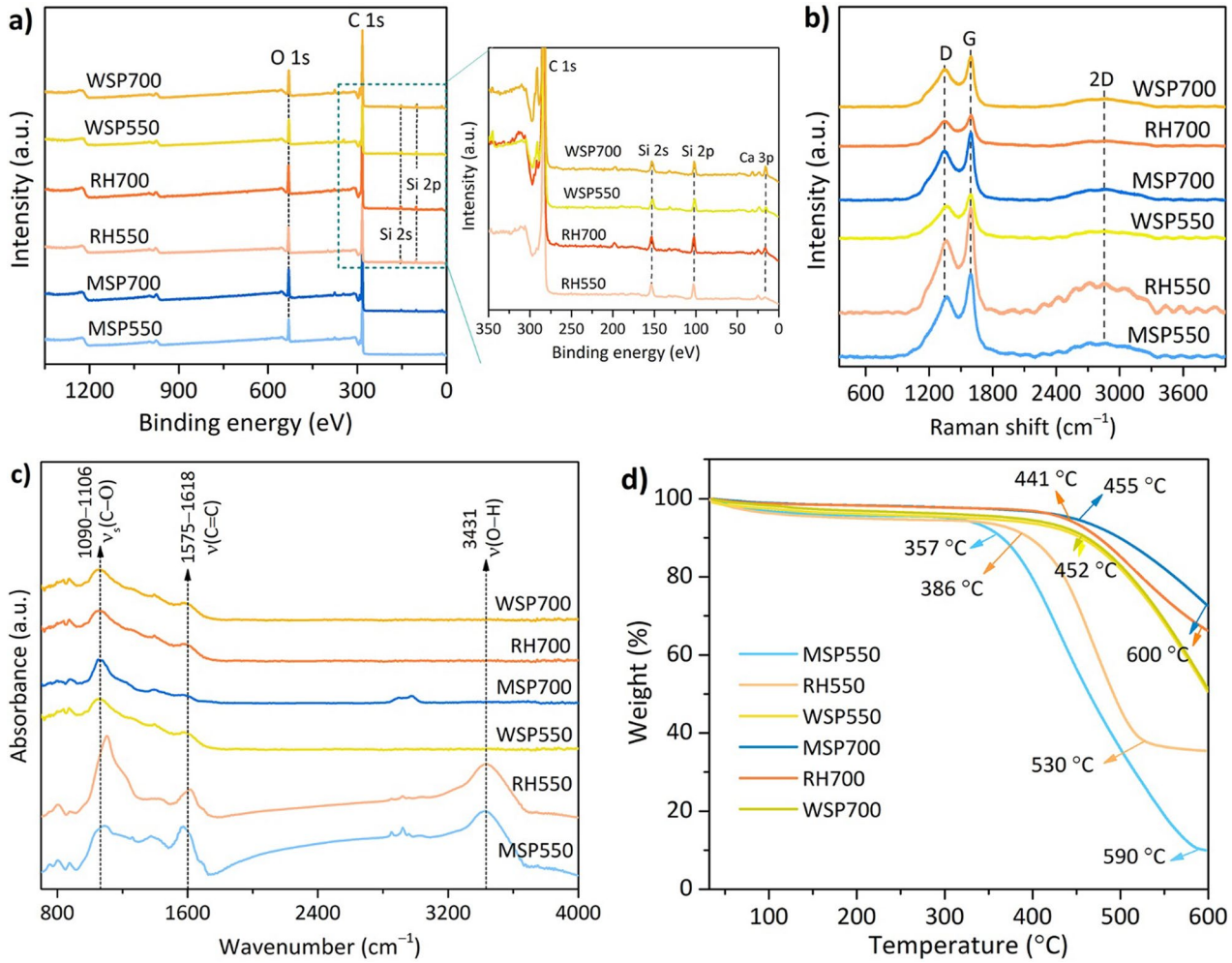

Fig. 4 Structural, chemical, and thermal stability properties of the standard biochars. **a** XPS survey result, **b** Raman spectra, **c** FTIR spectra, and **d** TGA curves for standard biochar pyrolyzed at 550 and 700 °C

However, the intensities of these bands exhibited a gradual decline, with a near-complete disappearance observed at approximately 3431 cm^{-1} for WSP550 and all biochars prepared at 700 °C. This signified a reduction in the number of acidic groups (CO–, COOH, CHO stretching, and phenolic – OH stretching) with increasing pyrolysis temperature. In addition, the reflection of both basic and acidic groups of aromatic C=O rings at approximately 1614 cm^{-1} mostly vanished across all biochar samples (except for MSP550 and RH550). This result was highly consistent with the pore characteristics of WSP550, in which the wheat straw exhibited pyrolysis at ≥ 500 °C. The reduction of such reactive functional groups in WSP550 can likely promote the PCM uptake capacity owing to the advantages of reducing intermolecular interactions between the guest and host materials. In addition to the structural and microstructural properties of the biochar materials, their thermal stability is vital for guest-material adsorption, and the TGA thermograms are provided in Fig. 4d. The carbon materials demonstrated high stability, as evidenced by decomposition temperature ranges of 357–590, 386–530, 441–600, and 455–600 °C for MSP550, RH550, RH700, and MSP700, respectively. This decomposition can be attributed to the degradation of organic molecules, such as hemicelluloses, cellulose, and lignin, present in the biomaterials (Pariyar et al. 2020). In addition, minor degradation was observed at approximately 30–60 °C for RH550 and MSP550 owing to the exclusion of impurities, including moisture/water, due to the inherent hygroscopic characteristics of the biomass. Comparatively, WSP550 and WSP700 exhibited high thermal stability (degradation between 452 and 600 °C due to the decomposition of the organic matter (such as lignin)) (Cao et al. 2019), which is

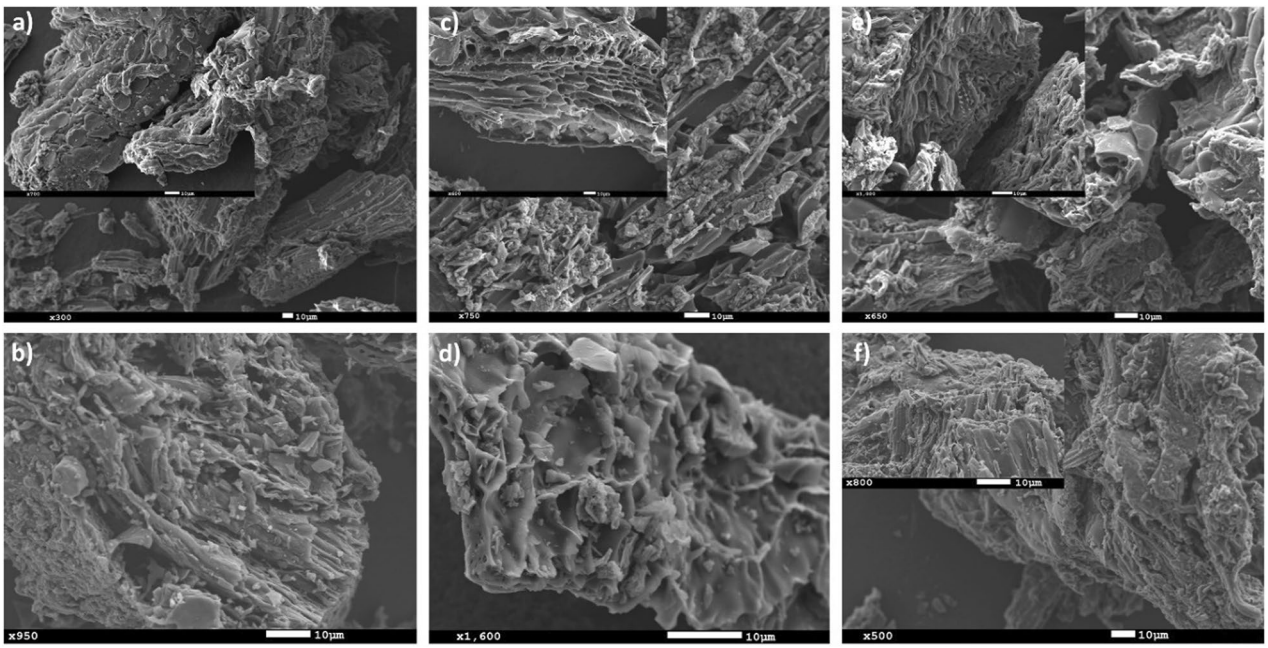

Fig. 5 SEM images of (**a**) MSP550/HXD, **b** MSP700/HXD, **c** RH550/HXD, **d** RH700/HXD, **e** WSP550/HXD, and **f** WSP700/HXD

a property similar to their highest biochar carbon stability, which was 96.51 ± 0.3% on a C-basis.

3.2 Structural and morphological properties of the biochar-based composite

Figure 5a–f displays SEM images of the biochar after impregnation with HXD. The rough surface was attributed to biochar, whereas the smooth surface was HXD. As shown in the SEM images, HXD firmly infiltrated the pores of the biochar matrices and displayed a thick microstructure owing to the surface tension and capillary force between the HXD molecules and the supporting materials. The HXD molecules were well-distributed throughout the biochar matrix. In contrast, the partial magnification of RH550 displayed comparatively vacant pores, primarily due to the weak affinity of RH550 for HXD (Fig. 5c). This leads to reduced adsorption in the pores, which could become vacant after the phase change process. This resulted in a lower encapsulation ratio and energy storage density.

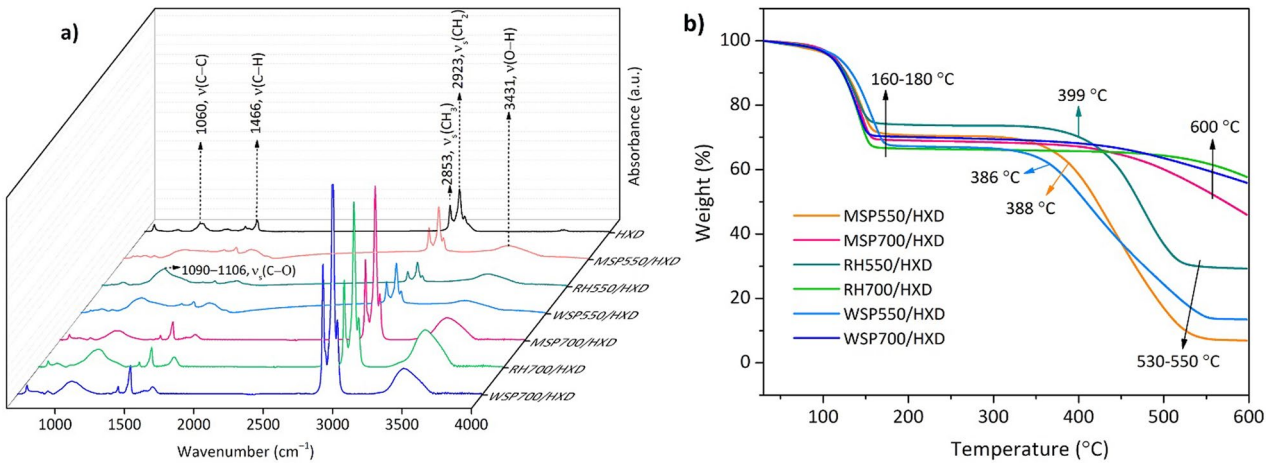

Fig. 6 Structural characteristics of the biochar-based composite PCMs. **a** FTIR spectra of pure hexadecane and the composite PCMs. **b** TGA thermograms of the bio-based composite samples

Additionally, the chemical properties of the biochar and HXD integration were assessed using FTIR spectroscopy. As presented in Fig. 6a, all biochar composites displayed the combined spectra of biochar and HXD without significant shifts in the main absorption peaks or new absorption peaks, demonstrating physical adsorption between HXD and the biochar materials. All composite materials exhibited prominent $-CH_3$ and $-CH_2-$ symmetric and asymmetric stretching vibrations of HXD at approximately 2853 and 2923 cm^{-1}, respectively. The characteristic peak at 1466 cm^{-1} corresponds to C–H bonds (CH_2 in-plane bending vibrations). The peaks at 1090–1106 cm^{-1} can be attributed to C–O–C stretching vibrations derived from the biochar-supporting matrix. Although the prominent distinctive peaks of HXD were displayed together in the FTIR spectra of the composite materials, the absorption peak intensities differed from those of pristine HXD and the other two biochar composite materials, presumably due to the limited amount of HXD infiltration inside the biochar pores.

The thermal strengths of the as-fabricated phase-change hybrids were investigated using TGA (Fig. 6b). All composite materials exhibited analogous two-step thermal decomposition characteristics without substantial weight degradation detected at a temperature of less than 120 °C. The first decomposition step occurred from approximately 120 to 180 °C owing to the decomposition and evaporation of HXD and weight losses of 28.9%, 30.5%, 25.8%, 33.2%, 32.7%, and 29.6% for MSP550/HXD, MSP700/HXD, RH550/HXD, RH700/HXD, WSP550/HXD, and WSP700/HXD, respectively, which was consistent with the weight portion of HXD in the composites. The second step occurred from approximately 386 to 600 °C, equivalent to the decomposition of organic molecules from the biochar samples. Evidently, the weight loss revealed the HXD loading content inside the biochar samples, as a higher HXD loading content provides a phase-change composite with a stronger thermal energy density performance (Zhou et al. 2023). This further indicates that RH700 demonstrated the highest HXD loading content, which was attributed to its highest BET SSA (74.66 $m^2\ g^{-1}$) and cumulative mesopore volume (0.078 $cm^3\ g^{-1}$). It is also worth noting that RH550/HXD exhibited a distinct and higher thermal stability curve (from around 180 to 600 °C) compared to other biochar materials produced at 550 °C pyrolysis. This is likely due to the presence of high Si and other metals, as RH550 exhibited high Si content (3.9%), which may stabilize carbon more effectively than other forms of carbon components (Guo and Chen 2014). Meanwhile, WSP550/HXD exhibited a high PCM adsorption capacity, which was consistent with its structural properties (large pore diameter of 9.53 nm). Notably, pores that are larger than or match the size of the guest species can improve the encapsulation capability of biochar materials. In this regard, WSP550 had a higher pore size compared with that of the guest HXD (dimension of 2.36 nm and breadth of ~0.4 nm) (Martin et al. 1998). In contrast, supporting materials with pore sizes ranging from 0.5 to 2.4 nm render the guest materials inaccessible or dynamically limited for adsorption, resulting in a molecular sieve effect (Zhang et al. 2022a). Therefore, the HXD inside the biochar network was preserved from leaching to a certain extent. Therefore, the fabricated composite materials exhibited better thermal performance than the pure HXD.

3.3 Phase-change properties of biochar-based composite materials

Thermal parameters, such as the phase-transition enthalpy and phase-transition temperature of the bulk HXD and biochar–HXD composites, were assessed using DSC during both the melting and freezing processes. As shown in Fig. 7a, all hybrid materials displayed distinct melting and freezing phase-transition peaks. The fusion enthalpy (ΔH_m) and freezing enthalpy (ΔH_f) of pristine HXD were 251.1 and 249.6 J g^{-1}, correspondingly. As presented in Fig. 7b, MSP550/HXD, MSP700/HXD, RH550/HXD, RH700/HXD, WSP550/HXD, and WSP700/HXD displayed $\Delta H_m/\Delta H_c$ values of 61.9/61.1 J g^{-1}, 63.2/62.3 J g^{-1}, 59.6/59.1 J g^{-1}, 70.0/69.6 J g^{-1}, 64.6/64.0 J g^{-1}, and 58.1/57.7 J g^{-1}, correspondingly. Their enthalpy storage capacities were still lower than the latent heat storage capacity of pristine HXD owing to the interference of biochar, which showed no phase-transition behavior during the phase-change process; this is unavoidable. The melting temperature (T_m) and crystalline temperature (T_c) of all composite samples were 22.4 ± 0.6 and 11.3 ± 0.6 °C, respectively. Unlike other biochar composites (MSP550/HXD, MSP700/HXD, WSP550/HXD, and WSP700/HXD), the T_c slightly increased from 10.7 °C in RH550/HXD to 10.9 °C in RH700/HXD, indicating the relatively easy arrangement of regular molecular chains and improved crystal growth as the adsorption mesopore volume increased from 0.058 to 0.078 $cm^3\ g^{-1}$. This can lead to an improvement in the phase-transition enthalpy and phase-change temperature of the rice-husk-based composite as the temperature increases. In contrast, the T_c of wheat straw biomass decreased by 0.8 °C. Additionally, the encapsulation ratio (ω) of HXD in the composite PCMs was evaluated according to Eq. (1):

$$\omega = \frac{\Delta H_{m.comp.}}{\Delta H_{m.HXD}} \times 100\% \quad (1)$$

where $\Delta H_{m.comp.}$ and $\Delta H_{m.HXD}$ represent the fusion enthalpies of the phase-change composite and pure HXD,

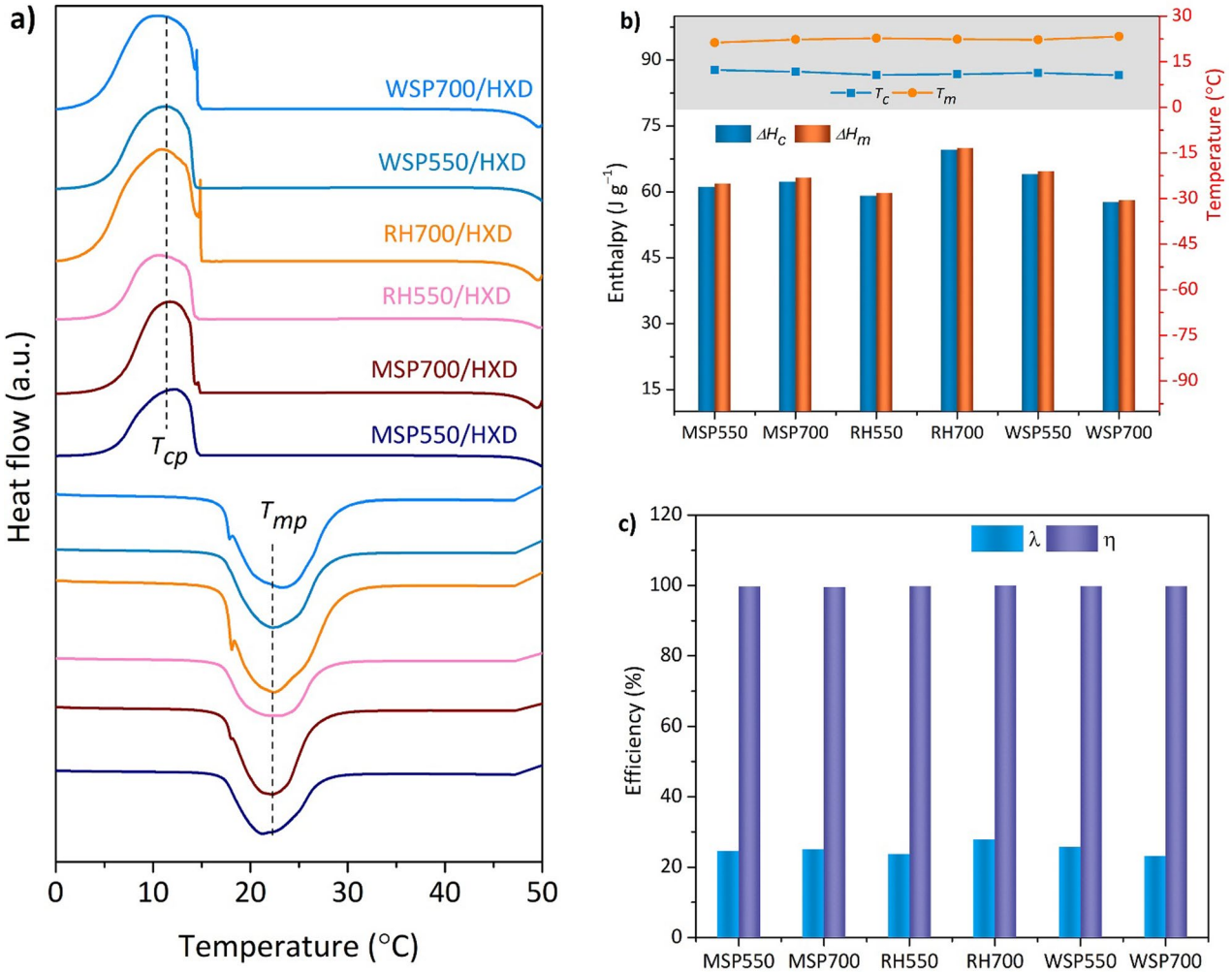

Fig. 7 Thermal properties of the fabricated composite samples. **a** DSC curves, **b** phase-transition enthalpy and phase-transition temperature of the prepared samples, and (**c**) enthalpy efficiency and relative enthalpy efficiency of the biochar composite samples

respectively. Hence, the ω values of HXD in MSP550/HXD, MSP700/HXD, RH550/HXD, RH700/HXD, WSP550/HXD, and WSP700/HXD were 24.6%, 25.2%, 23.8%, 27.9%, 25.7%, and 23.2%, respectively. Supporting materials with high SSAs provide various active sites for the adsorption of large guest molecules via surface- or interface-related interactions. In this context, RH700 provided a favorable BET SSA, thereby exhibiting a high energy storage capacity and ω. In view of the weight fraction, the enthalpy per unit mass of HXD in RH700/HXD (70.0/0.279 = 250.9 J g^{-1}) was nearly similar to that of the pristine PCM. This implies that the integration of HXD and biochar can exploit the characteristics of HXD to the greatest extent possible (Zhao et al. 2024). In contrast to other biochar-based composites that exhibited high energy storage density at 700 °C, the enthalpy storage density of WSP700/HXD was faintly lower than that of WSP550/HXD, presumably due to the high pyrolysis temperature causing disrupted pore channels and leading to the notably reduced SSA (7.35 m^2 g^{-1}). Pores with smaller kinetic diameters likely interact (including chemical bonding interactions) with guest materials/PCMs, leading to a reduced energy storage density (Zhang et al. 2022a).

In addition, the energy storage density and freedom-movement degree of HXD inside the as-prepared composite samples could be evaluated using the latent heat efficiency (λ) and relative latent heat efficiency (η). Typically, the higher the λ and η values, the higher the thermal energy storage density (Liu et al. 2023). The λ and η values of all samples were calculated according to Eqs. (2) and (3):

$$\lambda = \frac{\Delta H_{m(comp.)} + \Delta H_{f(comp.)}}{\left(\Delta H_{m(HXD)} + \Delta H_{f(HXD)}\right)} \times 100\% \quad (2)$$

$$\eta = \frac{\Delta H_{m(comp.)} + \Delta H_{f(comp.)}}{(\Delta H_{m.HXD} + \Delta H_{f.HXD}) \times \omega} \times 100\% \quad (3)$$

where $\Delta H_{f.comp.}$ and $\Delta H_{f.HXD}$ represent the crystalline enthalpies of the as-fabricated biochar-based phase-change composite and pristine HXD, respectively. The λ of the composite materials was close to the ω of the corresponding biochar-based samples. The η values of MSP550/HXD (99.7%), MSP700/HXD (99.5%), RH500/HXD (99.8%), WSP550/HXD (99.8%), and WSP700/HXD (99.8%) were lower than 100% (Fig. 7c), indicating the confinement effect of biochar materials regarding the free movement of HXD during the phase-change process. Conversely, the η of RH700/HXD (100%) reached 100%, indicating good thermal storage performance and relatively improved PCM movement (Hu et al. 2024). Additionally, the surface functionality (predominantly carboxyl and hydroxyl groups) and pore characteristics of biochar materials can also play significant roles in the thermal properties of composite materials. Strong confinement inside the supporting materials/biochar affects the encapsulation conformation of the PCM chains and the nucleation and crystal growth of the PCM molecules (Wang et al. 2016). For example, RH550 yielded a reduced phase-change enthalpy compared to RH700 due to the insufficient pore diameter and relatively "interactive" interaction between biochar functional groups and the inert HXD. This interaction restricts the movement of the HXD chain and impedes the crystallization of HXD in the biochar networks (Fig. 8). Hence, the latent heat efficiency and thermal performance of composite materials can largely depend on the biomass materials and synthesis conditions, such as the pyrolysis temperature.

In addition, for practical operations, the thermal performance of the designed composite should be preserved over an extended period. Therefore, a thermal cycling test over 500 cycles was conducted using a thermal cycler from 0 to 50 °C for composite materials prepared using 550 °C biochars, and the phase transition was evaluated using DSC (Fig. 9a). The phase-change temperature points minimally shifted, demonstrating high thermal reliability over repeated thermal cycles. The $\Delta H_m/\Delta H_c$ values of MSP550/HXD, RH550/HXD, and WSP550/HXD were 56.0/54.9, 51.8/50.8, and 59.3/58.5 J g^{-1}, correspondingly, with latent heat retention capacities of 90.5%, 86.7%, and 91.7%, respectively (Fig. 9b). This signified high HXD preservation in the biochar channels after multiple thermal cycles.

Furthermore, the seepage-resistance capability/shape stability characteristics of the as-synthesized composite materials were assessed using a hot-stage digital camera method wherein the samples were placed in a heating oven at 60 °C for over 30 min. The changes were recorded using a digital camera. The seepage test of pristine HXD was not incorporated because the sample was originally observed in a liquid state (Fig. 9c). As shown in Fig. 9d, no indication of liquid flow was observed in any of the biochar-supported HXD composite materials, indicating the enhanced form steadiness of the synthesized materials.

To demonstrate the energy conversion capability and internal homogeneity of the biochar-based phase-change energy storage, an infrared (IR) thermography evaluation was performed, revealing the dynamic thermal characteristics. To evaluate the performance of biomass pyrolyzed at a lower temperature (550 °C), composite materials of the same weight (approximately 0.71 mg), such as MSP550/HXD, RH550/HXD, and WSP550/HXD, were selected and subjected to IR irradiation. The changes were documented via an IR camera after 1 h of heating and cooling in the temperature series of 25 (room temperature) to 50 °C (Fig. 10a). During the heating stage, all samples exhibited nearly the same isothermal heating rate, whereas WSP550/HXD and RH550/HXD displayed relatively higher heating temperatures after 10 min of heating (Fig. 10b), presumably owing to the higher heat transfer performance of the supporting biomaterials. During the crystalline process, the temperature of the biocomposite decreased to ambient

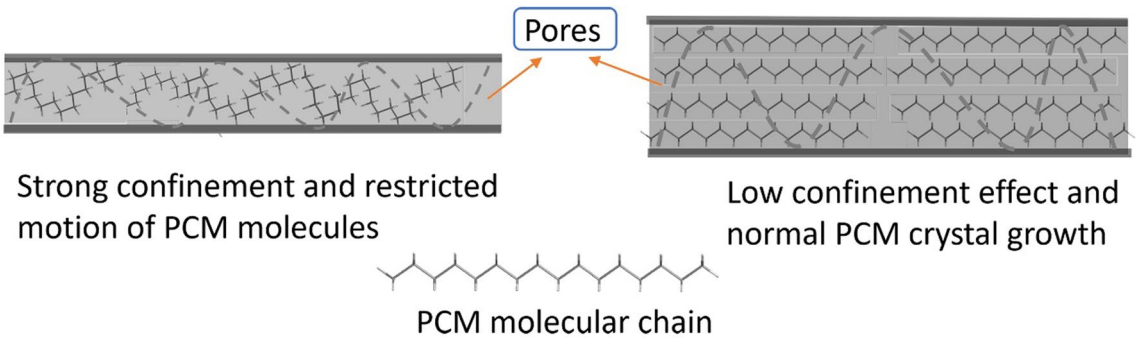

Fig. 8 Schematic illustration of PCM molecular chain confinement and adsorption conformation inside the biochar channels

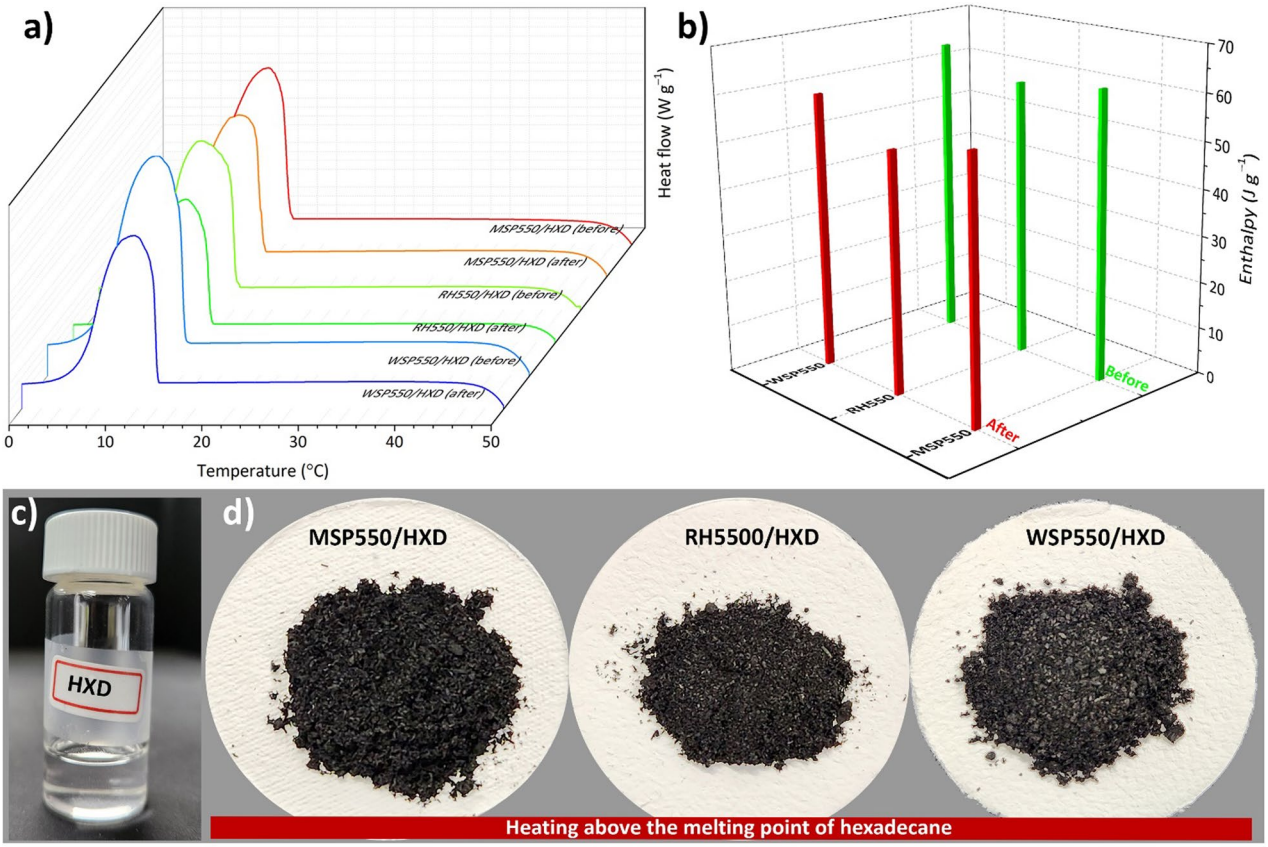

Fig. 9 Thermal reliability of the composite materials: (**a**) DSC curves and (**b**) phase-change enthalpy of the composite materials after and before 500 heating–cooling cycles. **c** Pristine hexadecane and (**b**) leakage test of the biochar composites at 60 °C via heating for over 30 min

temperature (20–40 °C) after 5 min. In this context, the as-prepared composite materials maintained their temperature for a relatively longer cooling time compared to composites fabricated using highly thermally conductive materials (e.g., boron nitride), which exhibited a temperature decrease within 10 s (Wang et al. 2019). To further confirm its application potential, the thermal transport performance of as-synthesized composite materials was evaluated, revealing thermal resistances of 0.5585, 0.5487, and 0.5339 (m^2·K) W^{-1} for MSP550/HXD, RH550/HXD, and WSP550/HXD, respectively. This further suggested the significant potential of these materials in thermal insulation applications. Additionally, the thermal performances of the as-prepared composite PCMs were highly competitive and even more advanced compared to those of recently documented composite materials, as shown in Fig. 10c, d and Table 2. This difference in the thermal performance of certain composite materials is due to the introduction of activating agents and biochar engineering materials, which improve the structural diversity responsible for the adsorption of the PCMs.

Furthermore, the as-prepared biochar-based composites, operating within an ambient temperature range of 20–40 °C and exhibiting promising energy storage capacity (60–65 J g^{-1}), can find application in low-carbon energy buildings, such as free-cooling ventilation systems and indoor thermal control applications. It can enhance the energy-saving capacity, thermal performance, and service life of buildings (Liu et al. 2024). As indicated above, the as-prepared phase-change composite exhibited a thermal resistance capability ranging from 0.5339 to 0.5585 (m^2·K) W^{-1}, indicating favorable building temperature regulation and reduced building energy consumption. It can be used to keep against heat dissipation and improve the energy storage density of target applications. For example, biochar-based phase change composite integrated with artificial stone, which is used for building finishing materials, demonstrated a temperature delay effect (of ~ 2.7 h), reduced peak temperature up to 5 °C, lowered the thermal conductivity by 0.65 W (m $K)^{-1}$, and improved thermal energy efficiency and indoor temperature control (Kim et al. 2021). Meanwhile, the as-prepared biochar-based composites exhibited prolonged

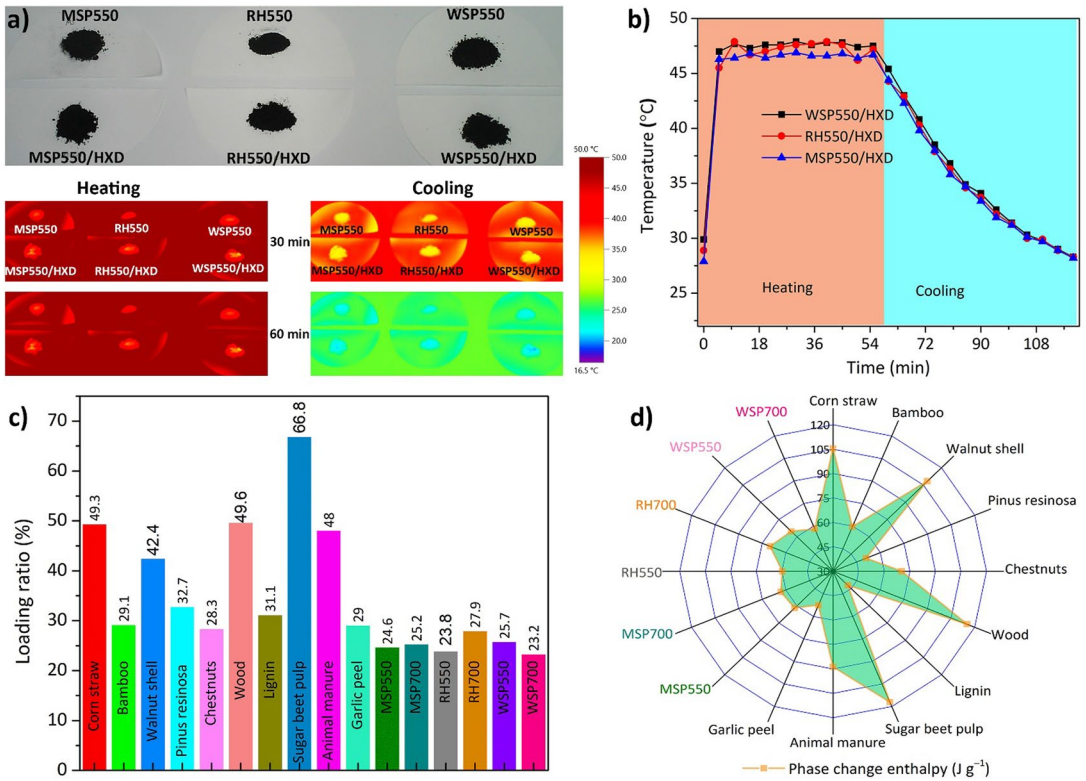

Fig. 10 Thermal management of the biochar-based composites. **a** IR images and (**b**) dynamic thermal performance of the biochar and biochar-based phase-change composites. The comparative thermal performances of the as-synthesized hybrids and other biochar-based composite PCMs are shown. **c** Encapsulation ratio and (**d**) phase-change enthalpy storage density

Table 2 Thermal performance comparison of the as-prepared composite and documented composite PCMs

Biomass feedstocks	PCMs	Loading ratio (%)	ΔH_m (J g^{-1})	ΔH_c (J g^{-1})	Refs.
Carbonized hazelnut wood	Capric acid	63.4	136.7	136.7	Hekimoğlu et al. (2021a)
Corn straw	Polyethylene glycol (PEG)	49.3	105.4	95.49	Liu et al. (2022b)
Walnut shell	Methyl palmitate	42.4	108.3	107.0	Hekimoğlu et al. (2021c)
Pinus resinosa	Dodecanoic acid	32.7	50.9	~50.3	Mandal et al. (2022)
Lemon peel	Heptadecane	64.7	141.8	–	Hekimoğlu et al. (2021b)
Sugar beet pulp	Capric-stearic acid	66.8	117.0	113.0	Sarı et al. (2022)
Chestnuts	Octadecane	28.3	70.2	66.1	Zhao et al. (2021)
Wood	Nonadecane	49.6	115.1	114.9	Hekimoğlu et al. (2023)
Lignin	PEG/polyvinyl alcohol	31.1	42.2	37.9	Niu et al. (2022)
Bamboo	Paraffin	38.8	79.4	78.8	Yue et al. (2023)
Bamboo	Paraffin	29.1	59.5	56.6	Yue et al. (2023)
Animal manure	Octadecane	48.0	88.7	89.0	Atinafu et al. (2024)
Garlic peel	Paraffin	29.0	52.5	51.9	Luo et al. (2022)
MSP550	Hexadecane	24.6	61.9	61.1	This study
MSP700	Hexadecane	25.2	63.2	62.3	This study
RH550	Hexadecane	23.8	59.6	59.1	This study
RH700	Hexadecane	27.9	70.0	69.6	This study
WSP550	Hexadecane	25.7	64.6	64.0	This study
WSP700	Hexadecane	23.2	58.1	57.7	This study

cooling and heating time, which is imperative to reduce energy consumption, minimize indoor air temperature variations, and preserve indoor thermal comfort. Additionally, a proper amount of biochar (approximately 4% of cement weight) ensures enhanced mechanical properties (strength), which further offers environmental benefits through recycling the waste. This provides abundant prospects for developing "green" passive energy infrastructure in building constructions.

Moreover, the enhanced characteristics of as-prepared composites, such as leakage-resistance capability and low extent of supercooling (< 13.0 °C) can project high-performance thermal management systems in the human thermal comfort zone. This will further broaden the application of biochar databases in renewable energy storage material development.

4 Conclusions

In summary, high-performance and eco-friendly phase-change composites are crucial for achieving high energy storage densities and utilization efficiencies. Phase-change composites composed of organic PCMs and three biochar matrices were formed at different carbonization temperatures. The thermal properties of the phase-change composites, in which HXD molecules are infiltrated, were assessed by calculating the phase-transition enthalpy and phase-transition temperature using DSC, and by evaluating thermal stability using TGA. The results displayed that the encapsulation ratio and phase-transition enthalpy increased with an increase in the textural properties of the biochars, such as the SSA and mesopore volume. RH700/HXD exhibited high phase-change enthalpy (70.0 J g^{-1}), which was 15% higher than that of the composites derived from RH550 due to a large SSA and cumulative mesopore volume. Concurrently, the phase-change enthalpy of the Miscanthus straw-derived biochar-based composites increased with increasing biochar preparation temperature. Conversely, WSP700/HXD exhibited the lowest enthalpy (58.1 J g^{-1}) owing to the lowest SSA at high temperatures, causing structural damage and complete pyrolysis. The pyrolysis temperature and feedstock used meaningfully affected the structural architecture of the biochar materials. All phase-change composites demonstrated optimal shape stability (60 °C, above the fusion temperature of pristine HXD), notable thermal stability, and durability. Additionally, the composites exhibited high latent heat efficiency (99.5–100%), with RH700/HXD showing superior capacity and maintaining high phase-change enthalpy retention, ranging from 86.7 to 91.7%, even after 500 heating–cooling cycles. Under similar pyrolysis conditions (550 °C), the composite materials exhibited thermal resistance ranging from 0.5339 (m^2·K) W^{-1} to 0.5585 (m^2·K) W^{-1}. This showcases the potential of the composite for thermal insulation, contributing to building energy savings. The results enabled us to report an additional understanding of the competitive influence of pore volume and SSA on the energy storage density and phase-change temperature owing to the pyrolysis temperature effect. Therefore, monitoring the pyrolysis temperature according to the biomass type and target application is suggested. Accordingly, this study offers a promising avenue for fabricating green, economical, and high-performance bio-based energy material composites for diverse renewable energy storage, harvesting, and utilizations, such as free-cooling ventilation systems in lightweight buildings.

Supplementary Information

The online version contains supplementary material available at https://doi.org/10.1007/s42773-024-00396-1.

Supplementary Material 1.

Acknowledgements
Not applicable.

Author contributions
Writing – original draft, Conceptualization: Dimberu G. Atinafu. Visualization, Investigation: Ji Yong Choi. Methodology: Jihee Nam. Writing – review & editing: Yujin Kang. Supervision, Funding acquisition: Sumin Kim. All authors read and approved the final manuscript.

Funding
This study was supported by the National Research Foundation of Korea (NRF) grant funded by the Korean Government (MSIT) (No. 2022R1A2C3008559). This research was supported by Yonsei 'Eokkaedongmu Project' through the 4th BK21 Graduate School Innovation Support Project funded by the Ministry of Education.

Data availability
The datasets used or analyzed during the current study are available from the corresponding author upon reasonable request.

Declarations

Competing interests
The authors declare that they have no known competing financial interests or personal relationships that could have appeared to influence the work reported in this paper.

Author details
[1]Department of Architecture and Architectural Engineering, Yonsei University, Seoul 03722, Republic of Korea.

Received: 5 June 2024 Revised: 15 October 2024 Accepted: 23 October 2024
Published online: 20 January 2025

References

Al-Ahmed A, Mazumder MAJ, Salhi B, Sari A, Afzaal M, Al-Sulaiman FA (2021) Effects of carbon-based fillers on thermal properties of fatty acids and their eutectics as phase change materials used for thermal energy

storage: a review. J Energy Storage 35:102329. https://doi.org/10.1016/j.est.2021.102329
Ali HM, Rehman T, Arıcı M, Said Z, Duraković B, Mohammed HI et al (2024) Advances in thermal energy storage: fundamentals and applications. Progr Energy Combust Sci 100:101109. https://doi.org/10.1016/j.pecs.2023.101109
Atinafu DG, Wi S, Yun BY, Kim S (2020) Engineering biochar with multiwalled carbon nanotube for efficient phase change material encapsulation and thermal energy storage. Energy 216:119294. https://doi.org/10.1016/j.energy.2020.119294
Atinafu DG, Choi JY, Yun BY, Nam J, Kim HB, Kim S (2024) Energy storage and key derives of octadecane thermal stability during phase change assembly with animal manure-derived biochar. Environ Res 240:117405. https://doi.org/10.1016/j.envres.2023.117405
Bordoloi U, Das D, Kashyap D, Patwa D, Bora P, Muigai HH, Kalita P (2022) Synthesis and comparative analysis of biochar based form-stable phase change materials for thermal management of buildings. J Energy Storage 55:105801. https://doi.org/10.1016/j.est.2022.105801
Cao Y, Shen G, Zhang Y, Gao C, Li Y, Zhang P et al (2019) Impacts of carbonization temperature on the Pb(II) adsorption by wheat straw-derived biochar and related mechanism. Sci Total Environ 692:479–489. https://doi.org/10.1016/j.scitotenv.2019.07.102
Chun Y, Sheng G, Chiou CT, Xing B (2004) Compositions and sorptive properties of crop residue-derived chars. Environ Sci Technol 38(17):4649–4655. https://doi.org/10.1021/es035034w
Edeh IG, Masek O, Fusseis F (2023) 4D structural changes and pore network model of biomass during pyrolysis. Sci Rep 13(1):22863. https://doi.org/10.1038/s41598-023-49919-z
Foong SY, Liew RK, Yuh Yek PN, Chan YH, Lam SS (2024) A review in production of nitrogen-enriched carbon materials via chitin pyrolysis and activation for enhanced wastewater remediation. Curr Opin Green Sustain Chem 47:100920. https://doi.org/10.1016/j.cogsc.2024.100920
Freeman TB, Foster KEO, Troxler CJ, Irvin CW, Aday A, Boetcher SKS et al (2023) Advanced materials and additive manufacturing for phase change thermal energy storage and management: a review. Adv Energy Mater 13(24):2204208. https://doi.org/10.1002/aenm.202204208
Guo J, Chen B (2014) Insights on the molecular mechanism for the recalcitrance of biochars: interactive effects of carbon and silicon components. Environ Sci Technol 48(16):9103–9112. https://doi.org/10.1021/es405647e
Haghighi Mood S, Pelaez-Samaniego MR, Garcia-Perez M (2022) Perspectives of engineered biochar for environmental applications: a review. Energy Fuels 36(15):7940–7986. https://doi.org/10.1021/acs.energyfuels.2c01201
Hekimoğlu G, Sarı A, Kar T, Keleş S, Kaygusuz K, Yıldırım N et al (2021a) Carbonized waste hazelnut wood-based shape-stable composite phase change materials for thermal management implementations. Int J Energy Res 45(7):10271–10284. https://doi.org/10.1002/er.6514
Hekimoğlu G, Sarı A, Arunachalam S, Arslanoğlu H, Gencel O (2021b) Porous biochar/heptadecane composite phase change material with leak-proof, high thermal energy storage capacity and enhanced thermal conductivity. Powder Technol 394:1017–1025. https://doi.org/10.1016/j.powtec.2021.09.030
Hekimoğlu G, Sarı A, Kar T, Keleş S, Kaygusuz K, Tyagi VV et al (2021c) Walnut shell derived bio-carbon/methyl palmitate as novel composite phase change material with enhanced thermal energy storage properties. J Energy Storage 35:102288. https://doi.org/10.1016/j.est.2021.102288
Hekimoğlu G, Sarı A, Gencel O, Tyagi VV, Sharma RK (2023) Activated carbon/expanded graphite hybrid structure for development of nonadecane based composite PCM with excellent shape stability, enhanced thermal conductivity and heat charging-discharging performance. Thermal Sci Eng Progr 44:102081. https://doi.org/10.1016/j.tsep.2023.102081
Hu B, Guo H, Cui Y, Li J, Cao M, Qi W et al (2024) Engineering multifunctional phase change composites enabled by dual-interpenetrating hybrid scaffold for excellent thermal conductivity and electromagnetic absorption. Chem Eng J 492:152259. https://doi.org/10.1016/j.cej.2024.152259
Igalavithana AD, Choi SW, Dissanayake PD, Shang J, Wang C-H, Yang X et al (2020) Gasification biochar from biowaste (food waste and wood waste) for effective CO_2 adsorption. J Hazardous Mater 391:121147. https://doi.org/10.1016/j.jhazmat.2019.121147
Jing J, Liu H, Wang X (2023) Long-term infrared stealth by sandwich-like phase-change composites at elevated temperatures via synergistic emissivity and thermal regulation. Adv Funct Mater 34:2309269. https://doi.org/10.1002/adfm.202309269
Kalu S, Seppänen A, Mganga KZ, Sietiö O-M, Glaser B, Karhu K (2024) Biochar reduced the mineralization of native and added soil organic carbon: evidence of negative priming and enhanced microbial carbon use efficiency. Biochar 6(1):7. https://doi.org/10.1007/s42773-023-00294-y
Kim YU, Yun BY, Nam J, Choi JY, Wi S, Kim S (2021) Evaluation of thermal properties of phase change material-integrated artificial stone according to biochar loading content. Construct Build Mater 305:124682. https://doi.org/10.1016/j.conbuildmat.2021.124682
Kong L, Wang Z, Kong X, Wang L, Ji Z, Wang X, Zhang X (2021) Large-scale fabrication of form-stable phase change nanotube composite for photothermal/electrothermal energy conversion and storage. ACS Appl Mater Interfaces. https://doi.org/10.1021/acsami.1c07160
Leng L, Xiong Q, Yang L, Li H, Zhou Y, Zhang W et al (2021) An overview on engineering the surface area and porosity of biochar. Sci Total Environ 763:144204. https://doi.org/10.1016/j.scitotenv.2020.144204
Li X, Liu Y, Xu Y, Tao P, Deng T (2023a) Solid–liquid phase change composite materials for direct solar-thermal energy harvesting and storage. Accounts Mater Res 4(6):484–495. https://doi.org/10.1021/accountsmr.2c00251
Li Y-R, Li Y-M, Hu W-J, Wang D-Y (2023b) Shaped photothermal conversion phase-change materials with excellent electromagnetic shielding performance and flame retardancy. Adv Eng Mater 25(14):2201885. https://doi.org/10.1002/adem.202201885
Liang Q, Pan D, Zhang X (2023) Construction and application of biochar-based composite phase change materials. Chem Eng J 453:139441. https://doi.org/10.1016/j.cej.2022.139441
Liu W-J, Jiang H, Yu H-Q (2015) Development of biochar-based functional materials: toward a sustainable platform carbon material. Chem Rev 115(22):12251–12285. https://doi.org/10.1021/acs.chemrev.5b00195
Liu H, Su S, Wang H, Wang M, Zhang S, Chang B, Yang B (2022a) A sustainable one-step strategy for highly graphitized capacitive carbons with hierarchical micro–meso–macro porosity. Nanoscale Adv 4(5):1394–1407. https://doi.org/10.1039/D1NA00856K
Liu S, Peng S, Zhang B, Xue B, Yang Z, Wang S, Xu G (2022b) Effects of biochar pyrolysis temperature on thermal properties of polyethylene glycol/biochar composites as shape-stable biocomposite phase change materials. RSC Adv 12(16):9587–9598. https://doi.org/10.1039/D1RA09167K
Liu S, Quan B, Sheng M, Yang Y, Hu X, Zhu C et al (2023) A novel in-situ growth ZIF-67 on biological porous carbon encapsulated phase change composites with electromagnetic interference shielding and multifunctional energy conversion. Nano Energy 114:108669. https://doi.org/10.1016/j.nanoen.2023.108669
Liu B, Lv G, Liu T, Liu M, Bian J, Sun Q, Liao L (2024) Research progress of biomass materials in the application of organic phase change energy storage materials. J Mater Chem A 12(15):8663–8682. https://doi.org/10.1039/D3TA07521D
Luo Y, Zhang F, Li C, Cai J (2022) Biomass-based shape-stable phase change materials supported by garlic peel-derived porous carbon for thermal energy storage. J Energy Storage 46:103929. https://doi.org/10.1016/j.est.2021.103929
Lv L, Wang J, Ji M, Zhang Y, Huang S, Cen K, Zhou H (2022) Effect of structural characteristics and surface functional groups of biochar on thermal properties of different organic phase change materials: dominant encapsulation mechanisms. Renewable Energy 195:1238–1252. https://doi.org/10.1016/j.renene.2022.06.117
Mandal S, Ishak S, Lee D-E, Park T (2022) Optimization of eco-friendly Pinus resinosa biochar-dodecanoic acid phase change composite for the cleaner environment. J Energy Storage 55:105414. https://doi.org/10.1016/j.est.2022.105414
Martin DS, Weightman P, Gauntlett JT (1998) The evaporation of *n*-hexadecane from highly oriented pyrolytic graphite studied by atomic force microscopy. Surf Sci 417(2):390–405. https://doi.org/10.1016/S0039-6028(98)00717-1
Mašek O, Buss W, Roy-Poirier A, Lowe W, Peters C, Brownsort P et al (2018a) Consistency of biochar properties over time and production scales: a characterisation of standard materials. J Anal Appl Pyrolysis 132:200–210. https://doi.org/10.1016/j.jaap.2018.02.020
Mašek O, Buss W, Sohi S (2018b) Standard biochar materials. Environ Sci Technol 52(17):9543–9544. https://doi.org/10.1021/acs.est.8b04053

Matuszek K, Kar M, Pringle JM, MacFarlane DR (2023) Phase change materials for renewable energy storage at intermediate temperatures. Chem Rev 123(1):491–514. https://doi.org/10.1021/acs.chemrev.2c00407

Montoya J, Pecha B, Janna FC, Garcia-Perez M (2017) Identification of the fractions responsible for morphology conservation in lignocellulosic pyrolysis: visualization studies of sugarcane bagasse and its pseudo-components. J Anal Appl Pyrolysis 123:307–318. https://doi.org/10.1016/j.jaap.2016.11.015

Niu L, Li X, Zhang Y, Yang H, Feng J, Liu Z (2022) Electrospun lignin-based phase-change nanofiber films for solar energy storage. ACS Sustain Chem Eng 10(39):13081–13090. https://doi.org/10.1021/acssuschemeng.2c03462

Pariyar P, Kumari K, Jain MK, Jadhao PS (2020) Evaluation of change in biochar properties derived from different feedstock and pyrolysis temperature for environmental and agricultural application. Sci Total Environ 713:136433. https://doi.org/10.1016/j.scitotenv.2019.136433

Qian T, Li J, Min X, Deng Y, Guan W, Ning L (2016) Radial-like mesoporous silica sphere: a promising new candidate of supporting material for storage of low-, middle-, and high-temperature heat. Energy 112:1074–1083. https://doi.org/10.1016/j.energy.2016.07.023

Qiu J, Huo D, Xia Y (2020) Phase-change materials for controlled release and related applications. Adv Mater 32:2000660. https://doi.org/10.1002/adma.202000660

Sarı A, Hekimoğlu G, Karabayır Y, Sharma RK, Arslanoğlu H, Gencel O, Tyagi VV (2022) Capric-stearic acid mixture impregnated carbonized waste sugar beet pulp as leak-resistive composite phase change material with effective thermal conductivity and thermal energy storage performance. Energy 247:123501. https://doi.org/10.1016/j.energy.2022.123501

Singh P, Sharma RK, Khalid M, Goyal R, Sarı A, Tyagi VV (2022) Evaluation of carbon based-supporting materials for developing form-stable organic phase change materials for thermal energy storage: a review. Solar Energy Mater Solar Cells 246:111896. https://doi.org/10.1016/j.solmat.2022.111896

Tomczyk A, Sokołowska Z, Boguta P (2020) Biochar physicochemical properties: pyrolysis temperature and feedstock kind effects. Rev Environ Sci Bio/technol 19(1):191–215. https://doi.org/10.1007/s11157-020-09523-3

Wan Z, Sun Y, Tsang DCW, Khan E, Yip ACK, Ng YH et al (2020) Customised fabrication of nitrogen-doped biochar for environmental and energy applications. Chem Eng J 401:126136. https://doi.org/10.1016/j.cej.2020.126136

Wang J, Yang M, Lu Y, Jin Z, Tan L, Gao H et al (2016) Surface functionalization engineering driven crystallization behavior of polyethylene glycol confined in mesoporous silica for shape-stabilized phase change materials. Nano Energy 19:78–87. https://doi.org/10.1016/j.nanoen.2015.11.001

Wang J, Liu D, Li Q, Chen C, Chen Z, Song P et al (2019) Lightweight, superelastic yet thermoconductive boron nitride nanocomposite aerogel for thermal energy regulation. ACS Nano 13(7):7860–7870. https://doi.org/10.1021/acsnano.9b02182

Wang Y, Zhang M, Shen X, Wang H, Wang H, Xia K et al (2021) Biomass-derived carbon materials: controllable preparation and versatile applications. Small 17(40):2008079. https://doi.org/10.1002/smll.202008079

Weidner MC, Evenson Z, Zamponi M, Possart W (2019) Molecular motion in viscous DGEBA with nanoparticles as seen by quasi-elastic neutron scattering. Macromol Chem Phys 220(1):1800275. https://doi.org/10.1002/macp.201800275

Xie Y, Xiao S, Chen W, Hu X, Liu Y, Jiang L et al (2024) Shape-stabilized nanosilver-modified grapefruit peel-based porous carbon composite phase change material with high thermal conductivity, photothermal conversion performance and thermal management capability. J Energy Storage 83:110819. https://doi.org/10.1016/j.est.2024.110819

Xiong T, Ok YS, Dissanayake PD, Tsang DCW, Kim S, Kua HW, Shah KW (2022) Preparation and thermal conductivity enhancement of a paraffin wax-based composite phase change material doped with garlic stem biochar microparticles. Sci Total Environ 827:154341. https://doi.org/10.1016/j.scitotenv.2022.154341

Yadav A, Pandey AK, Samykano M, Kareri T, Tyagi VV (2024) Wheat husk derived microparticle infused organic phase change material for efficient heat transfer and sustainable thermal energy storage. J Energy Storage 86:111204. https://doi.org/10.1016/j.est.2024.111204

Yang R, Guo X, Wu H, Kang W, Song K, Li Y et al (2022) Anisotropic hemp-stem-derived biochar supported phase change materials with efficient solar-thermal energy conversion and storage. Biochar 4(1):38. https://doi.org/10.1007/s42773-022-00162-1

Yu S, He J, Zhang Z, Sun Z, Xie M, Xu Y et al (2024) Towards negative emissions: hydrothermal carbonization of biomass for sustainable carbon materials. Adv Mater 36:2307412. https://doi.org/10.1002/adma.202307412

Yuan Y, Sun X, Yang M, Xu F, Lin Z, Zhao X et al (2017) Stiff, thermally stable and highly anisotropic wood-derived carbon composite monoliths for electromagnetic interference shielding. ACS Appl Mater Interfaces 9(25):21371–21381. https://doi.org/10.1021/acsami.7b04523

Yuan X, Cao Y, Li J, Patel AK, Dong C-D, Jin X et al (2023) Recent advancements and challenges in emerging applications of biochar-based catalysts. Biotechnol Adv 67:108181. https://doi.org/10.1016/j.biotechadv.2023.108181

Yuan X, Suvarna M, Lim JY, Pérez-Ramírez J, Wang X, Ok YS (2024) Active learning-based guided synthesis of engineered biochar for CO_2 capture. Environ Sci Technol 58(15):6628–6636. https://doi.org/10.1021/acs.est.3c10922

Yue X, Zhang R, Jin X, Zhang X, Bao G, Qin D (2023) Bamboo-derived phase change material with hierarchical structure for thermal energy storage of building. J Energy Storage 62:106911. https://doi.org/10.1016/j.est.2023.106911

Zeng Y, Zhang F, Wu J, Huang J (2023) Green pepper-derived hierarchical porous carbon for supercapacitors with high performance. Mater Adv 4(9):2192–2200. https://doi.org/10.1039/D3MA00045A

Zhang Z, Wang J, Tang X, Liu Y, Han Z, Chen Y (2019) Comparison study between mesoporous silica nanoscale microsphere and active carbon used as the matrix of shape-stabilized phase change material. Sci Rep 9(1):16056. https://doi.org/10.1038/s41598-019-52553-3

Zhang S, Zheng M, Tang Y, Zang R, Zhang X, Huang X et al (2022a) Understanding synthesis–structure–performance correlations of nanoarchitectured activated carbons for electrochemical applications and carbon capture. Adv Funct Mater 32(40):2204714. https://doi.org/10.1002/adfm.202204714

Zhang Y, He M, Wang L, Yan J, Ma B, Zhu X et al (2022b) Biochar as construction materials for achieving carbon neutrality. Biochar 4(1):59. https://doi.org/10.1007/s42773-022-00182-x

Zhao J, Jiang Y, Fan H, Liu M, Zhuo O, Wang X et al (2017) Porous 3D few-layer graphene-like carbon for ultrahigh-power supercapacitors with well-defined structure-performance relationship. Adv Mater 29(11):1604569. https://doi.org/10.1002/adma.201604569

Zhao P-P, Deng C, Zhao Z-Y, Lu P, He S, Wang Y-Z (2021) Hypophosphite tailored graphitized hierarchical porous biochar toward highly efficient solar thermal energy harvesting and stable storage/release. Chem Eng J 420:129942. https://doi.org/10.1016/j.cej.2021.129942

Zhao J, Zhang W, Lu Q, Liao T, Li W, Zhang X, Li Q (2024) High energy-capacity and multiresponsive phase change fibers via in situ polymer composition with expanded carbon nanotube networks. Chem Eng J 481:148262. https://doi.org/10.1016/j.cej.2023.148262

Zhou Y, Zeng J, Guo Y, Chen H, Bi T, Lin Q (2023) Three-dimensional hierarchical porous carbon surface-decorated graphitic carbon foam/stearic acid composite as high-performance shape-stabilized phase change material with desirable photothermal conversion efficiency. Appl Energy 352:121995. https://doi.org/10.1016/j.apenergy.2023.121995